X-RAY ANALYSIS OF CREEP-INDUCED LOCAL LATTICE PARAMETER CHANGES IN A MONOCRYSTALLINE NICKEL-BASE SUPERALLOY

H. Mughrabi, H. Biermann and T. Ungár*

Institut für Werkstoffwissenschaften, Universität Erlangen-Nürnberg,
D-W 8520 Erlangen, F.R. Germany,

*)Institute for General Physics, Eötvös University, H-1445 Budapest, Hungary.

Abstract

The γ/γ'-lattice mismatch of specimens of the monocrystalline nickel-base superalloy SRR 99 has been measured by a high-resolution X-ray diffraction technique for the undeformed state and after high-temperature creep deformation. During creep deformation beyond the minimum creep rate (total strain $\approx$ 0.5 %), the lattice mismatches, measured in and perpendicular to the [001] stress axis, respectively, undergo changes in opposite directions. This reflects the build-up of a complex deformation-induced triaxial state of internal stress in the phases γ and γ'. The overall resolved shear stresses which act in γ' and γ due to the combined action of the external and internal stresses are estimated and the conditions under which cutting of the γ'-phase by dislocations should occur are discussed.

Superalloys 1992
Edited by S.D. Antolovich, R.W. Stusrud, R.A. MacKay,
D.L. Anton, T. Khan, R.D. Kissinger, D.L. Klarstrom
The Minerals, Metals & Materials Society, 1992

Introduction and Objectives

Monocrystalline nickel-base superalloys with high γ'-volume fraction have become increasingly important as modern turbine-blade materials. At high temperatures and under the action of an external or internal stress the microstructure changes from cuboidal γ'-precipitates to a raft-like γ/γ'-structure, e.g. (1-4). Important factors which influence this microstructural change are the direction of external load and the sign and magnitude of the lattice mismatch, $\delta = 2(a_{\gamma'} - a_\gamma)/(a_{\gamma'} + a_\gamma)$, defined as the relative difference of the lattice parameters of the phases γ' and γ, $a_{\gamma'}$ and a_γ, respectively. In the past, the γ/γ'-lattice mismatch has been investigated by different techniques, compare e.g. (5-11).

The aim of the present work is to obtain reliable data about the local distribution of the lattice parameters of the phases γ and γ' and the lattice mismatch δ of the monocrystalline nickel-base superalloy SRR 99 after high-temperature creep deformation. For this purpose X-ray line profiles were measured with negligible instrumental line broadening and evaluated in order to obtain the deformation-induced residual long-range internal stresses. From the superposition of the latter with the external stress, the resolved shear stresses acting in the slip systems of the type $\{111\}\langle\bar{1}01\rangle$ in the phases γ and γ' are calculated and discussed with respect to the deformation behaviour.

Experimental

Samples

Samples of the monocrystalline nickel-base superalloy SRR 99 with rod axes near [001] were investigated. In the initial state the alloy is composed of a fcc γ-matrix and of ordered $L1_2$ γ'-precipitates which are arranged in cubes of about 0.25 to 0.3 μm mean edge size with faces perpendicular to the $\langle 100\rangle$-directions. The samples were standard heat-treated by a single-stage annealing of 16h/860°C. The γ'-volume fraction was determined as 71 $\pm$ 2 % by analysis of X-ray line profiles of creep-deformed samples which were separated into γ- and γ'-subprofiles, taking into account the different atomic scattering factors of the phases. This result was confirmed by complementary techniques.

The samples were creep-deformed in tension at constant stresses σ between 150 MPa and 750 MPa at temperatures of 750°C, 900°C and 1050°C (12,13). The data from several specimens which were crept to rupture are given in Table I (12). All specimens were cooled to room-temperature by air blow to the grips immediately after fracture. One further set of samples was deformed at T = 900°C and σ = 305 MPa to different total strains ϵ (sample (a): undeformed, samples (b) to (e) correspond to ϵ = 0.5 %, 1.5 %, 3.0 % and 21.3 %, respectively (12)). In all samples creep-deformed till rupture either at 1050°C or at 900°C under stresses of 305 MPa and 444 MPa, a raft-like γ/γ'-structure had developed. The other samples still had a cuboidal γ'-structure even at the end of creep deformation.

X-ray diffraction technique

From the creep-deformed specimens {001}-oriented slices were cut by spark erosion and polished. One type of specimen examined was cut perpendicular to the [001]-direction of the stress axis and investigated with the (002) Bragg reflection ('axial case'). The other type of specimen was perpendicular to the [010]- (equivalent to [100])-direction and was studied with the (020)/(200) Bragg reflection ('side case'). The X-ray line profiles were measured with monochromatic $Cu_{K\alpha 1}$-radiation, using a special double-crystal diffractometer with high angular resolution and negligible instrumental line broadening (10,11). The specimens were rotated continuously around the exact Bragg angle to probe the exact lattice parameter distribution of the sample (10). The fact that the line profiles were not broadened due to instrumental effects was confirmed by the observation that the {002} and {004}-type line profiles had identical shapes. The absolute Bragg angles (and lattice parameters) were evaluated using a high-purity nickel single crystal as a reference. The reported values were calculated as a mean value from at least four line profiles.

Table I: Data from creep tests (12).

sample	T/°C	σ/MPa	E/GPa	ϵ_f/%	t_f/h	$\dot{\epsilon}_{ss}/s^{-1}$
1	1050	150	86.0	13.2	133.6	$3.0 \cdot 10^{-7}$
2	1050	200	86.0	19.4	31.9	$1.2 \cdot 10^{-6}$
3	1050	305	84.9	25.0	2.8	$3.0 \cdot 10^{-5}$
4	900	305	98.1	21.3	515,5	$1.2 \cdot 10^{-7}$
5	900	444	104.5	28.7	89.3	$7.0 \cdot 10^{-7}$
6	900	444	98.0	30.0	83.2	$7.1 \cdot 10^{-7}$
7	900	607	96.6	24.2	6.7	$6.8 \cdot 10^{-6}$
8	900	607	97.5	25.1	10.0	$6.5 \cdot 10^{-6}$
9	900	750	98.5	24.4	0.7	$7.0 \cdot 10^{-5}$
10	750	750	109.6	22.4	1348.3	$2.8 \cdot 10^{-8}$
11*	750	750	109.6	19.7	400.8	$1.3 \cdot 10^{-7}$

The values of Young's modulus E were calculated for the slightly differing orientations using the appropriate high-temperature elastic constants which had been reported by Kuhn and Sockel (14) for an alloy similar to SRR 99.
ϵ_f: strain to failure, t_f: time to failure, $\dot{\epsilon}_{ss}$: quasi steady-state creep rate.
* This sample has been predeformed in tensile creep at T = 900°C, σ = 305 MPa, to a strain of 3 % and annealed for 10 min. at 1080°C in order to obtain a raft structure prior to the creep test.

Results

Samples creep-deformed at 1050°C

First, a short review of earlier results obtained on samples which were creep-deformed at 1050°C (10) is given in order to compare these data subsequently with results of creep deformation at different temperatures. Fig. 1 shows typical line profiles of alloy SRR 99 a) in the initial standard heat-treated state and b) after creep deformation and cooling to room temperature. The (002) line profile of the undeformed sample which is indistinguishable from the (200) and (020) profiles shows a pronounced asymmetry on the left hand side. This is due to the smaller volume fraction and the larger lattice parameter of the γ-phase (i.e. negative "constrained" lattice mismatch in the undeformed state, $\delta_{undef} = -1.4 \cdot 10^{-3}$ (10)). Hence the maximum of the profile can be assigned mainly to the γ'-phase and the more slowly decreasing tail on the lower angle side to the γ-phase.

The X-ray line profiles of a sample creep-deformed at a constant stress of 305 MPa are shown in Fig. 1b (11). These profiles are broadened markedly in comparison with those of the undeformed sample and exhibit dramatically changed shapes. In the axial case the profile has a reversed asymmetry on the right-hand side and even shows a shoulder, whereas the (020) line profile (side case) shows the original asymmetry, which has, however, become more pronounced, as evidenced by the appearance of a second peak. The shape of line profiles of samples deformed at stresses of 150 MPa and 200 MPa are intermediate between those shown in Fig. 1a and b.

The profiles of the deformed samples can be separated by a 'mirror'-procedure (10), which yields the subprofiles of the phases γ and γ'. The result of this evaluation is that the centres of gravity of the subprofiles are shifted apart from each other in the side case, whereas they are shifted towards each other and even overlap in the axial case.

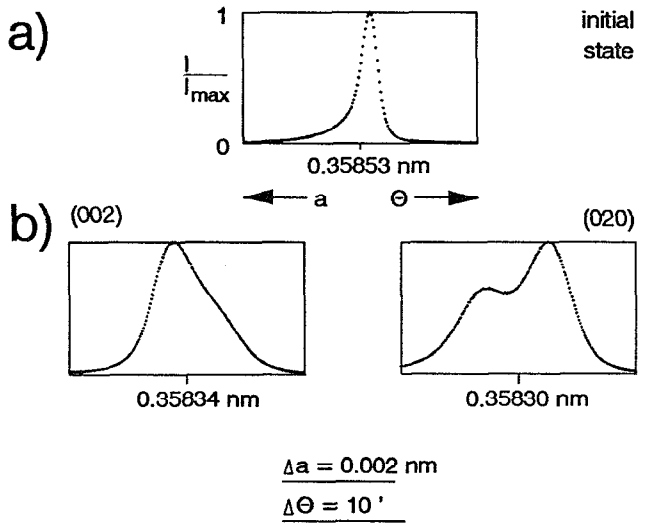

Figure 1: X–ray line profiles. (a) Undeformed state. (b) (002) and (020) Bragg reflections of the creep–deformed sample 3 (σ = 305 MPa at T = 1050°C) (11). The stated lattice parameters refer to the centres of gravity of the profiles.

As shown in Fig. 2a the lattice parameter of γ' in the [010]–direction, $a^{\gamma'}_{[010]}$, decreases with the applied stress, whereas the lattice parameter in the [001]–direction, $a^{\gamma'}_{[001]}$, increases. The strongest change of the lattice parameter is found for the γ–phase in the direction of the applied stress: $a^{\gamma}_{[001]}$ decreases by about 0.3 %. On the other hand, $a^{\gamma}_{[010]}$ shows only a small increase. It is evident that the mean lattice parameters evaluated from the centres of gravity of the line profiles decrease with increasing applied stress.

Samples creep–deformed at 900°C

Creep deformation to rupture at different stresses. The change of the line profiles of samples creep–deformed at 900°C (samples 4 to 9) with increasing applied stress is similar to that of samples deformed at the higher temperature. The profiles are, however, broadened more markedly and therefore more difficult to separate than the profiles of samples 1 to 3. The dependence of the lattice parameters as a function of the applied stress is given in Fig. 2b. The figure shows that $a^{\gamma}_{[001]}$ decreases considerably but not as strongly as after creep at 1050°C. The values of $a^{\gamma'}_{[001]}$ increase, the increase being slightly

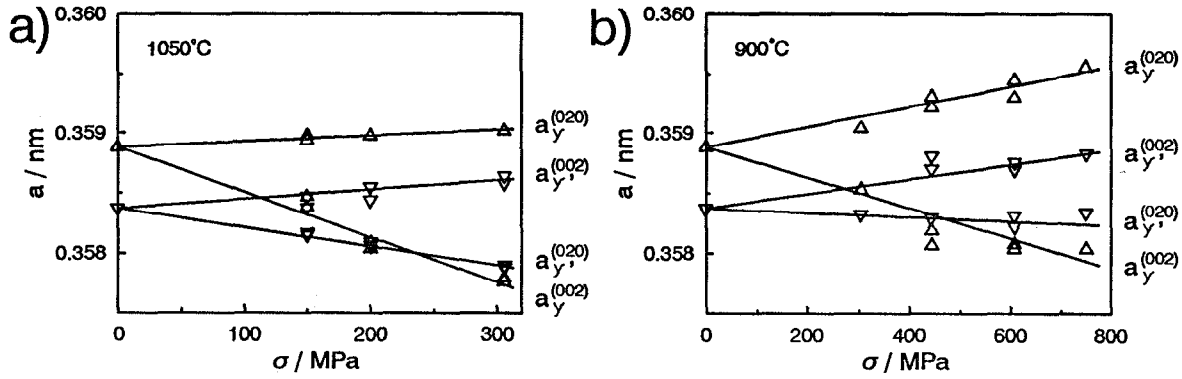

Figure 2: Lattice parameters of γ and γ' vs. applied stress for the (002)– and (020)–planes. (a) Samples 1 to 3, T = 1050°C (11). (b) Samples 4 to 9, T = 900°C.

stronger than that shown in Fig. 2a for samples crept at 1050°C. The (002)–profile (axial case) of the sample deformed at 305 MPa is nearly symmetrical. Therefore the stated lattice parameter represents the mean value obtained from the centre of gravity of the corresponding line profile. The lines represent a best fit to each set of data points. The (002) measurements for $\sigma = 444$ MPa were not included in these fits, since the only very slight asymmetry in the line profiles led to some uncertainty in the peak separation procedure. The (002) profiles of samples deformed at 607 MPa and 750 MPa are asymmetric, but due to their broadening they show no separate shoulders like sample 3 in Fig. 1b. The (020) line profiles (side case), however, always showed a separate shoulder, and the lattice parameter values obtained have a smaller error than those of the (002) profiles. In the axial case the lattice parameters of the γ–phase increase strongly in comparison to the 1050°C–data. The $a^{\gamma'}_{[001]}$–values decrease with increasing applied stress.

Creep–deformation at $\sigma = 305$ MPa to different strains. Fig. 3a shows the differentiated creep curve in a semi–logarithmic plot with a minimum creep rate at $\epsilon \approx 0.5$ % and a quasi steady–state (ss) regime beyond $\epsilon \approx 3$ %. Sample (a) represents the undeformed state, sample (b) was unloaded at the minimum of the creep rate. Samples (c) and (d) correspond to the strains at which raft formation begins and is completed, respectively. Sample (e) (identical to sample 4) was deformed to rupture.

The line profiles of sample (b) are indistinguishable from profiles of undeformed samples. At a strain of 1.5 % (sample (c)) the (002) profiles are symmetrical and the (020) profiles show a separate shoulder on the lower–angle side (Fig. 3b). The profiles of samples (c) to (e) do not differ significantly from one another.

Samples creep–deformed at 750°C

The two samples investigated at this temperature were deformed at a stress of $\sigma = 750$ MPa. One sample had a cuboidal γ' microstructure (sample 10) and one a pre–rafted microstructure (sample 11). The creep rate of the pre–rafted sample was found to be about one order of magnitude larger than that of the sample with the cuboidal γ/γ'–microstructure. The (002) line profiles of sample 10 show an asymmetry on the higher–angle side, the (020) line profiles a small asymmetry on the lower–angle side. The shape of the line profiles of the pre–rafted sample 11 is very different from that of sample 10. The (002) line profile has a second peak on the higher–angle side, whereas the (020) profile is

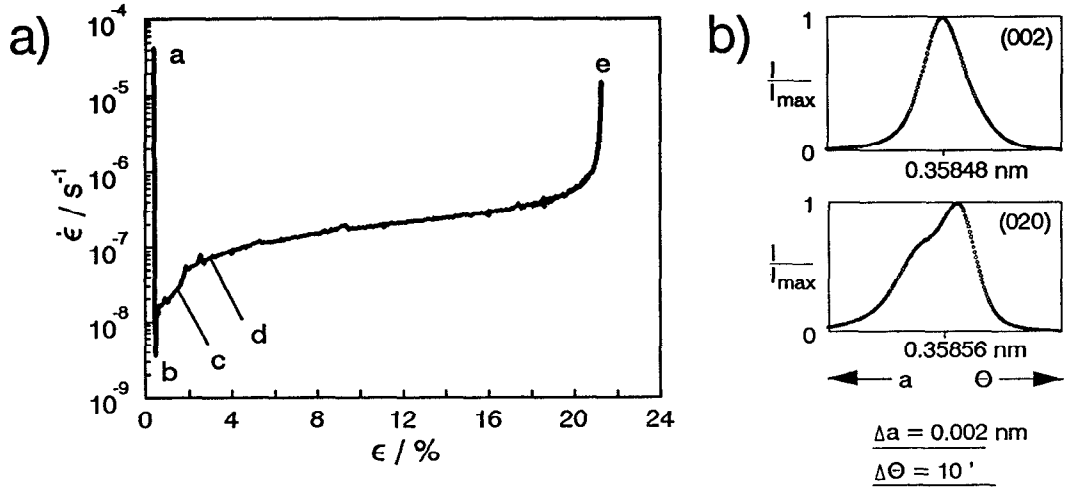

Figure 3: (a) Creep rate vs. strain of samples (b) to (e) deformed to different strains ϵ at $\sigma = 305$ MPa and T = 900°C (12). (b) X–ray line profiles of sample (e) ($\epsilon = 21.3$ %).

broadened markedly and nearly symmetrical. This (020) line profile can be separated into two subprofiles corresponding to the phases γ and γ'. The γ–subprofile is situated on the lower–angle side relative to the γ'–subprofile. The sense of the asymmetries of the two samples corresponds to that of samples 1 to 9. However, the magnitude of the shift of the subprofiles differs noticeably from that of the other samples.

Discussion

γ/γ'–lattice mismatch

Mismatch as a function of stress. In Fig. 4a and b the values of the so–called constrained lattice mismatch δ of samples deformed at 1050°C and 900°, measured at room temperature, are given as a function of applied stress. The mismatch of the undeformed state, $\delta_{\text{undef}} = -1.4 \cdot 10^{-3}$, was not evaluated from the line profiles but from so–called ω–2θ–scans of the intensity distribution in reciprocal space (10). The γ/γ'–lattice mismatch values of deformed samples were determined as $\delta_{[001]}$ and $\delta_{[010]}$ for the Bragg reflections (002) and (020) in the directions [001] and [010], respectively. Their dependence on the applied stress is shown in Fig. 4. The γ/γ'–mismatch shows a strong dependence on applied stress for the {002} lattice planes both parallel and perpendicular to the external stress axis. The mismatch of the side case in the [010]–direction, $\delta_{[010]}$, decreases slowly with increasing external stress. $\delta_{[001]}$ increases very strongly to $\delta_{[001]} \approx +2.4 \cdot 10^{-3}$ (T = 1050°C and σ = 305 MPa) and to $\delta_{[001]} \approx +2.2 \cdot 10^{-3}$ (T = 900°C and σ = 750 MPa). The values of $\delta_{[001]}$ for T = 1050°C, σ = 150 MPa (sample 1) and T = 900°C, σ = 305 MPa (sample 4) and 444 MPa (samples 5 and 6) cannot be given, because the profiles were either symmetrical (samples 1 and 4) or had only a small asymmetry (samples 5 and 6) and were therefore not separable. It is clear, however, that $\delta_{[001]}$ should be near zero in the cases T = 1050°C, σ = 150 MPa and T = 900°C, σ = 350 MPa in accordance with the dependence shown in Fig. 2. For the following evaluations $\delta_{[001]} = 0$ will be taken as an approximation in these cases. In the case of samples 5 and 6, $\delta_{[001]}$ is determined by interpolation to be $0.9 \cdot 10^{-3}$. The corresponding mismatch values of samples 10 and 11 (T = 750°C, σ = 750 MPa) were found to be $\delta_{[001]} = +2.4 \cdot 10^{-3}$ and $+4.9 \cdot 10^{-3}$ and $\delta_{[010]} = -1.8 \cdot 10^{-3}$ and $-3.3 \cdot 10^{-3}$, respectively.

Mismatch as a function of strain. The lattice mismatches $\delta_{[001]}$ and $\delta_{[010]}$ of sample (b) which was deformed to $\epsilon = 0.5$ % are both equal to the value $-1.4 \cdot 10^{-3}$ of the undeformed state. The (002) line profiles (axial case) of samples (c) to (e) are almost symmetrical and therefore not separable, the mismatch is about zero. In the side case, the lattice mismatches are $-1.90 \cdot 10^{-3}$, $-1.91 \cdot 10^{-3}$ and $-1.95 \cdot 10^{-3}$ for the strains of 1.5 %, 3 % and 21.3 %, respectively. These mismatch values are, within the scatter due to separation of the line profiles, constant in the range of strains from $\epsilon = 1.5$ % until rupture ($\epsilon = 21.3$ %).

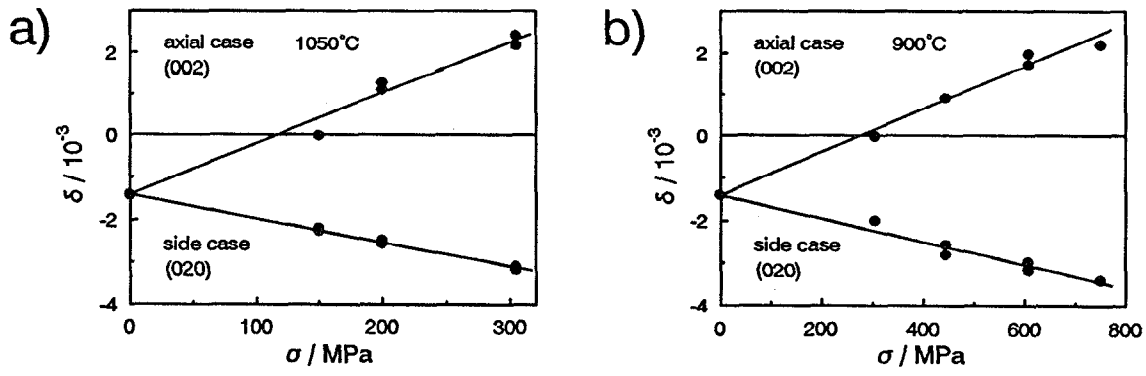

Figure 4: γ/γ'–lattice mismatch versus applied stress for (a) 1050°C (11) and (b) 900°C.

Deformation–induced residual long–range internal stresses

The shifts of the subprofiles and the change of the lattice parameters of the phases γ and γ' can be described in terms of residual long–range internal stresses, as explained by a composite model, cf. (10,11). In this model dislocations located in the γ/γ'–interfaces act as sources of internal stresses. In the unloaded state, the hard γ'–phase remains in a forward and the soft γ–phase in a backward stressed state with respect to the applied stress. The residual deformation–induced internal strains in the directions [001] and [010], $\epsilon_{[001]}$ and $\epsilon_{[010]}$, respectively, are evaluated from the deformation–induced changes of the lattice mismatch. Thus, the residual internal strain in the [001] direction is given by

$$\epsilon_{[001]} = \Delta(\delta)_{[001]} = \delta_{[001]} - \delta_{\text{undef.}} \tag{1}$$

For the strains in the [100] and/or [010]–directions analogous equations are valid. The difference between the internal stresses in the phases γ and γ' in the directions [001] and [010], $\Delta\sigma_{[001]}$ and $\Delta\sigma_{[010]}$, can be evaluated from the elastic deformation–induced internal strains in the phases γ and γ' via Hooke 's generalized law, e.g. for $\Delta\sigma_{[001]}$, as:

$$\Delta\sigma_{[001]} = \frac{E}{(1+\nu)(1-2\nu)} \cdot [(1-\nu)\epsilon_{[001]} + \nu(\epsilon_{[100]} + \epsilon_{[010]})], \tag{2}$$

where ν is Poisson's ratio. Here one must note that this is a simplified approach which does not take into account that, for the continuous phase (γ in cuboidal, γ' in raft structure), different stress states exist in the regions aligned roughly parallel and perpendicular to the stress axis (10). Stress equilibrium in the phases γ and γ' requires that the following relation holds between the local internal stresses $\Delta\sigma^{\gamma}$ and $\Delta\sigma^{\gamma'}$ (in a given direction) and the corresponding volume fractions f^{γ} and $f^{\gamma'}$ of the γ and γ'–phases, respectively:

$$\Delta\sigma^{\gamma} f^{\gamma} + \Delta\sigma^{\gamma'} f^{\gamma'} = 0. \tag{3}$$

Although the Young's moduli of the phases γ and γ' are different, the present work uses the Young's moduli of the alloy for simplicity. In order to relate the internal stresses to the deformation process, it would be necessary to determine their value at the temperature of deformation by taking into account also the effect of thermally induced stresses. However, since, at present, the significance of the latter is unclear, thermally induced stresses will be ignored in the present evaluation.

With the above equations the internal stresses in the phases γ and γ' in the directions [001] and [010] were calculated for the appropriate temperatures, using the relevant high temperature elastic data: Young's modulus E (see Table I), Poisson's ratio $\nu = 0.395$, 0.398 and 0.407 for T = 750°C, 900°C and 1050°C, respectively, (14). The internal stresses are compressive in γ along the [001]–direction and in γ' along the [010]–direction, and tensile in γ' along the [001]–direction and in γ along the [010]–direction. The largest internal stress prevails in γ along the direction of the applied stress: $\Delta\sigma^{\gamma}_{[001]} = -169$ MPa and -203 MPa for T = 900°C/σ = 750 MPa and 1050°C/σ = 305 MPa, respectively. In the case of samples deformed at 750°C the internal stresses are different from those of the other samples: tension prevails in the directions [001] and [010] in γ', compression in both directions in γ. In the pre–rafted sample (sample 11), deformed at 750°C, the internal stresses are larger than in the sample with the cuboidal γ/γ' structure deformed at the same stress. This is in contrast with the results of samples deformed at 1050°C with and without pre–deformation which show no difference from each other (11). In these latter samples, however, the microstructure at rupture is always raft–like.

The mismatch data of samples (a) and (b) to (e), crept at 900°C at a stress of 305 MPa to different strains, show that the residual internal stresses develop after the minimum of the creep rate at a strain of 0.5 %. During the subsequent deformation process the internal stresses do not change significantly beyond 1.5 % strain until rupture (sample (e)).

Resolved shear stresses

In the following, the procedure for calculating the overall resolved shear stresses acting in γ' (and in γ) is described. Approximations will be used where exact quantitative values are not available. The overall resolved shear stress τ on the stressed slip systems of the type $\{111\}\langle\bar{1}01\rangle$ due to the superposition of the external and the internal stresses can be evaluated by the following relation for the stress in the γ'–phase which is similar to an equation of Pollock and Argon (15):

$$\tau^{\gamma'}_{\{111\}\langle\bar{1}01\rangle} = (\sigma_{\text{applied}} + \Delta\sigma^{\gamma'}_{[001]} - \Delta\sigma^{\gamma'}_{[010]}) \cdot \frac{1}{\sqrt{6}} \qquad (4)$$

A similar relation holds for the stress in the γ–phase. In this expression, the initial coherency stresses of the originally cuboidal γ'–particles are explicitly omitted, assuming that these coherency stresses correspond to a triaxial tensile stress state without shear stresses. At any rate, the internal stresses in the γ'–phase should be small, mainly due to the high volume fraction of γ'. Therefore the evaluated resolved shear stresses in the γ'–phase are probably realistic approximations. In the case of the γ–phase equation 4 should be interpreted in terms of the following contributions (15): i) Coherency stresses, ii) Orowan stresses, iii) solid solution hardening and iv) dislocation dislocation interactions, including hardening effects of gliding dislocations with dislocation networks situated at the γ/γ'–phase boundaries. Such a detailed evaluation is beyond the scope of this paper.

The overall resolved shear stresses τ^{γ} and $\tau^{\gamma'}$ acting in the phases γ and γ', respectively, were determined as described above for all specimens investigated in this and in our earlier study (11) and are plotted as a function of the applied stress in Fig. 5a. From the comparison of the values $\tau^{\gamma'}$ with the critical resolved shear stress (crss) of the γ'–phase at the appropriate temperature and strain rate it should be possible to infer whether the γ'–phase has yielded and has been penetrated by dislocations. For this purpose, the $\tau^{\gamma'}$–data (and the τ^{γ}–data) are replotted in Fig. 5b as a function of the quasi–steady state creep rate $\dot{\epsilon}_{ss}$ (at the beginning of the almost steady–state creep) which is taken as the relevant creep rate. From this plot the locally acting shear stresses $\tau^{\gamma'}$ are extracted for some given values of $\dot{\epsilon}_{ss}$ and plotted as a function of temperature in Fig. 6. In this evaluation, the pre–rafted specimen 11 which exhibited a higher subsequent creep–rate (12,13) was also used, since there were no other creep data at 750°C available. The evaluated data are then compared with values from the literature on the crss–values of $Ni_3(Al,Ti)$ (16), which corresponds approximately to the γ'–phase, as a function of temperature and for given strain rates. In view of the phenomenon of flow stress asymmetry, it must be pointed out, however, that the data in ref. (16) refer to compression tests. This comparison, although crude, shows that the $\tau^{\gamma'}$–values do indeed lie in the range of the crss–values of $Ni_3(Al,Ti)$ reported for $\dot{\epsilon} = 5 \cdot 10^{-6}s^{-1}$.

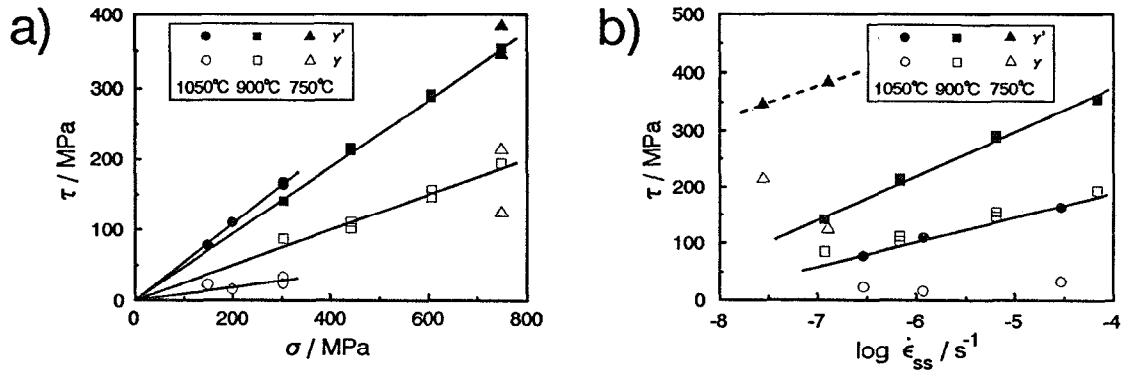

Figure 5: Local resolved shear stresses (a) in the phases γ and γ' vs. applied stress and (b) in the phase γ' as a function of the quasi stationary creep rate $\dot{\epsilon}_{ss}$.

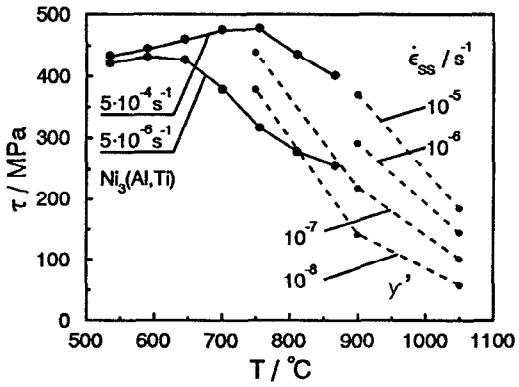

Figure 6: Critical resolved shear stress (in compression) of $Ni_3(Al,Ti)$ in the [001]–direction for strain rates of $5{\cdot}10^{-6}s^{-1}$ and $5{\cdot}10^{-4}s^{-1}$, respectively, (16) and local shear stresses in the γ'–phase in stressed glide systems of the type $\{111\}\langle\bar{1}01\rangle$.

Fig. 6 shows that the deformation of samples 10 and 11 at 750°C falls into a range of strain rate and stress, where the γ'–phase should be penetrated by dislocations. The shear stress in these samples is high enough to allow cutting, especially since the shear stress is higher than that necessary for cutting of $Ni_3(Al,Ti)$ at a higher strain rate. This statement is supported by TEM studies of these samples which show cutting of γ' with associated stacking faults (17). At the temperature of 900°C samples deformed at stresses of 607 MPa and 750 MPa (samples 7, 8 and 9) are also in that shear stress–temperature regime at the given strain rate, where cutting of γ' seems to be possible. Besides the approximations mentioned previously, our estimated data do not include the fact that the γ/γ'–phase boundaries are covered with dislocation networks which have a hardening effect. They also ignore that $Ni_3(Al,Ti)$ is not identical with γ' and do not take into account that there are local stress concentrations in the microstructure which could modify the actual local shear stresses (15). This is especially true in the cuboidal γ/γ'–microstructure. This factor, however, is more important for the γ–phase. Regarding the flow stress in the constrained γ–phase factors such as, in particular, the absolute value of the coherency stresses in the initial state are not yet known reliably. Hence, as already mentioned, a more detailed evaluation with respect to the different microstructural hardening contributions will not be attempted here.

Conclusions

1) In the undeformed state the monocrystalline alloy SRR 99 shows asymmetrical X–ray line profiles and has a negative lattice mismatch of $\delta_{\text{undef}} = -1.4 \cdot 10^{-3}$.
2) In [001]–oriented samples creep–deformed at stresses up to 750 MPa at different temperatures the (002) and the (020) line profiles are markedly different from each other. The asymmetry observed in the undeformed state is enlarged in the side case and *reversed* in the axial case.
3) The change of the lattice mismatch was evaluated in terms of long–range internal stresses. The deformation–induced internal stresses are triaxial. They build up after the minimum of the creep rate and remain constant during quasi steady–state creep until rupture.
4) The internal stresses of samples creep–deformed at 900°C and 1050°C depend linearly on the applied stress.
5) From the superposition of the triaxial internal stresses at the temperature of deformation and the applied external stress the overall resolved shear stresses on the active glide systems were evaluated.
6) The estimated resolved shear stresses acting in the γ'–phase were found to be comparable to the crss of $Ni_3(Al,Ti)$ for given strain rates.

Acknowledgment: The authors are very grateful to Dr. J. Hammer for providing the samples and to Dr. R. Keller for critical reading of the manuscript. The financial support of the Volkswagen–Stiftung is acknowledged gratefully (Az. I/65383).

References

(1) D. D. Pearson, F. D. Lemkey and B. H. Kear, "Stress Coarsening of γ' and its Influence on Creep Properties of a Single Crystal Superalloy", in 'Superalloys 1980', (eds. J. K. Tien, S. T. Wlodek, H. Morrow, M. Gell and G. E. Maurer), American Society for Metals, Metals Park, Ohio (1980), 513–520.

(2) R. A. MacKay and L. J. Ebert, "The Development of γ–γ' Lamellar Structures in a Nickel-Base Superalloy during Elevated Temperature Mechanical Testing", Met. Trans., 16A (1985), 1969-1982.

(3) C. Carry and J. L. Strudel, "Apparent and Effective Creep Parameters in Single Crystals of a Nickel Base Superalloy, Part II", Acta Met., 26 (1978), 859–870.

(4) P. Caron and T. Kahn, "Improvement of Creep Strength in a Nickel–base Single–crystal Superalloy by Heat Treatment", Mater. Sci. Eng., 61 (1983), 173–184.

(5) M. V. Nathal, R. A. MacKay and R. G. Garlick, "Temperature Dependence of γ–γ' Lattice Mismatch in Nickel–base Superalloys", Mater. Sci. Eng., 75 (1985), 195-205.

(6) A. Lasalmonie, J. L. Strudel, "Interfacial Dislocation Networks around γ' Precipitates in Nickel–Base Alloys", Phil. Mag., 32 (1975), 937-949.

(7) R. C. Ecob, M. P. Shaw, A. J. Porter and B. Ralph, "The Application of Convergent–Beam Electron Diffraction to the Detection of Small Symmetry Changes Accompanying Phase Transformations, Part I", Phil. Mag. A, 44 (1981), 1117-1133.

(8) D. Bellet and P. Bastie, "Temperature Dependence of the Lattice Parameter of the γ and γ' Phases in the Nickel–Based Superalloy CMSX-2. Part II: Neutron Diffraction Study of the Lattice Parameter Mismatch", Phil. Mag. B, 64 (1991), 143-152.

(9) L. Müller, T. Link and M. Feller–Kniepmeier, "Temperature Dependence of the Thermal Lattice Mismatch in a Single Crystal Nickel–Base Superalloy Measured by Neutron Diffraction", Scripta metall. et mater., 26 (1992), 1297–1302.

(10) H.–A. Kuhn, H. Biermann, T. Ungár and H. Mughrabi, "An X–Ray Study of Creep–Deformation Induced Changes of the Lattice Mismatch in the γ'–Hardened Monocrystalline Nickel–Base Superalloy SRR 99", Acta metall. et mater., 39 (1991), 2783-2794.

(11) H. Biermann, H.–A. Kuhn, T. Ungár, J. Hammer and H. Mughrabi, "Internal Stresses, Coherency Strains and Local Lattice Parameter Changes in a Creep–Deformed Monocrystalline Nickel–Base Superalloy", in 'Proc. 9th Int. Conf. on Strength of Metals and Alloys', 14th to 19th July 1991, Haifa, Israel, Vol. 1, (eds. D. G. Brandon, R. Chaim and A. Rosen), Freund Publ. Comp. Ltd. London, England (1991), 421–428.

(12) J. Hammer, Doctorate Thesis, Universität Erlangen–Nürnberg, (1990).

(13) J. Hammer and H. Mughrabi, "High–Temperature Creep and Microstructure of the Monocrystalline Nickel–Base Superalloy SRR 99", in 'Advanced Materials and Processes, Proc. of the First European Conf. on Advanced Materials and Processes', Aachen, Germany (edited by D. Driver and H. Mughrabi), DGM Informationsgesellschaft, Oberursel (1990), 445–450.

(14) H.-A. Kuhn and H. G. Sockel, "Contributions of the Different Phases of Two Nickel–Base Superalloys to the Elastic Behavior in a Wide Temperature Range", phys. stat. sol. (a), 119 (1990), 93-105.

(15) T. M. Pollock and A. S. Argon, "Creep Resistance of CMSX–3 Nickel Base Superalloy Single Crystals", Acta metall. et mater., 40 (1992), 1–30.

(16) G. R. Leverant, M. Gell and S. W. Hopkins, "The Effect of Strain Rate on the Flow Stress and Dislocation Behavior of a Precipitation–Hardened Nickel–Base Alloy", Mater. Sci. Eng., 8 (1971), 125-133.

(17) R. R. Keller, unpublished work (1992).